



For a ridge regularized linear readout model, we can directly compute the prior predictive distribution, which turns out to be a normal distribution with some covariance between the inputs. This predictive distribution is a full description of the inductive bias and generalization behavior of this linear readout model. By using a metric on these predictions, we get pseudo-metrics for representations, which characterize how well representations could be distinguished based on linear readouts from them. We first describe and analyze our new metric theoretically and then apply it to commonly used image processing models trained on ImageNet-1k for further evaluation.

## 2 Related Work

Here, we deal with the general question how to compare neural networks to each other. For this purpose, a neural network is a series of parameterized functions that are applied to an input and the outputs of previous functions. We call the outputs of these functions representations of the input. Different networks use different functions to create representations and generally have no corresponding parts or parameter values. Thus most comparisons are based on comparing representations rather than specifications of the functions themselves [9]. There are three major approaches to comparing models and their representations.

The first type of comparisons is based on comparing only the output of models. The immediate appeal of this approach is that all models for a specific task need to make predictions in the same format. Thus, models can be compared at this stage independent of their internal computations. The first metric for comparison is always overall performance. For detailed comparisons, an analysis of the errors can be more informative though [17, 18]. To enable comparisons of internal representations one can train a (usually linear or logistic) "probe" that predicts something based on the internal representation [19]. The results depend on the details of the evaluation task and on the training scheme for the readout though. To reduce the dependence on the exact task, a recent methods searches for the task with the most different results [20].

The second type of comparisons is based on (linearly) mapping one of the models to the other, which is known in neuroscience as an encoding model [11]. Comparisons based on fitting an explicit map are asymmetric by default. For some situations like predicting brain measurements based on a model representation, this is sensible. For comparisons between model representations, machine learning favors symmetric measures like variations of canonical correlation analysis [21, 22]. Ideally, we should aim for a metric though, such that our intuitions about similarity hold and clustering or embedding methods work effectively. This can be achieved by using generalized shape metrics [2].

The third type of comparisons is based on similarity structure. The first step of this approach is to compute a matrix of pairwise (dis-)similarities between stimuli or conditions for each model. These matrices can be compared directly. In neuroscience, this is known as representational similarity analysis [23]. In machine learning, this is based on the Kernel (similarity) matrix instead of the dissimilarity matrix and such methods are known as centered Kernel alignment [1]. The neuroscience and machine learning approaches are similar and, in some cases, exactly equivalent [24].

There are deep connections between these different approaches [9, 25]. Indeed, our metrics nicely connect the linear readout model to comparisons based on Kernel matrices and distances, because our metric depends only on the inner products between the representations of the inputs.

## 3 Methods

### 3.1 Bayesian comparison framework

We will apply Bayesian statistics to the (typically linear) models that are used to map representations to a task output (Fig. 1). Once we define a prior distribution over the weights, each representation then predicts a joint distribution of outputs for any set of stimuli. Formally, for a list of stimuli  $S = [s_1, \dots, s_n]$  represented by vectors  $x_i$ , and a potentially random readout function  $f_\theta$  from the space of representations into the space of outputs the probability of observing a specific vector of outputs  $y$  is:

$$p(y|S) = \int p(f_\theta(x) = y)p(\theta)d\theta \tag{1}$$

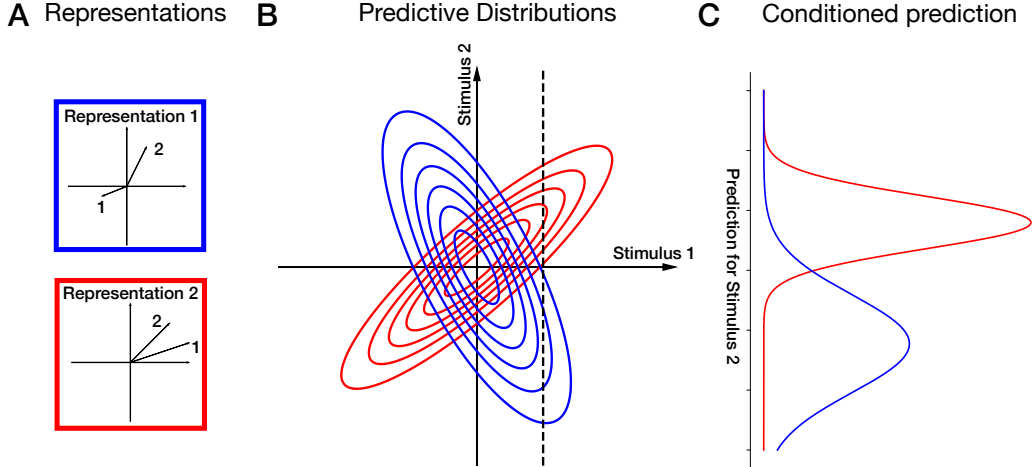


Figure 1: Minimal example for the Bayesian comparison framework: two stimuli in two 2D representations **A**: The original representations of the two stimuli. **B**: Predictive Distributions induced by a linear read out model with a zero mean Gaussian weight prior. These are the distributions we compare to determine the (dis-)similarity of representations. **C**: Prediction for Stimulus 2 according to the two models if a value of 1 for Stimulus 1 is given as training data. In the Bayesian statistics these are computed by conditioning the distribution in **B**.

To compare models to each other, we can apply a distance for probability distributions to the predictive distributions of the models. Such distances quantify how well the two distributions can be separated based on a random draw from them, i.e. how well one could tell which of the two models a random linear readout comes from. Additionally, the prior predictive distribution is a complete description of the generalization behavior of the model, i.e. of the inductive bias for any type of task a readout model might be trained for on the test stimuli.

### 3.2 Linear readout models

While our Bayesian Framework in theory supports any set of read out functions with a prior over them, we will focus on linear read outs with a isotropic Gaussian weight prior here. This setup is the Bayesian treatment for ridge regression with a fixed regularization strength.

Formally, the predictive distribution for a mean readout  $\bar{\mathbf{y}} \in \mathbb{R}^n$  for  $n$  stimuli with representations  $\mathbf{x}_i \in \mathbb{R}^k$  concatenated in a matrix of representations  $X \in \mathbb{R}^{k,n}$  with rows for each stimulus and columns for each feature dimension in the model is:

$$\bar{\mathbf{y}} = X\beta \quad \beta \sim N(0, \sigma_\beta^2 I) \quad (2)$$

As linear transformations of Gaussians are Gaussian, the distribution for  $\bar{\mathbf{y}}$  is then also a Gaussian with known parameters:

$$\bar{\mathbf{y}} \sim N(0, \sigma_\beta^2 X X^T) \quad (3)$$

With many stimuli or low-dimensional representations,  $X X^T$  can become rank deficient such that the predictive distributions for the mean degenerate. The natural solution for this problem is to take into account that measurements for a readout will be noisy and add independent Gaussian noise with standard deviation  $\sigma_\epsilon$  to each observation. The predictive distribution for observations  $\mathbf{y}$  then is:

$$\mathbf{y} \sim N(0, \sigma_\beta^2 X X^T + \sigma_\epsilon^2 I) \quad (4)$$

To properly fit a linear readout one would adjust  $\sigma_\beta$  to induce the right amount of regularization. When implementing this, we can compensate for any re-scaling of  $X$  or  $X X^T$  by adjusting  $\sigma_\beta$ . Thus,

we should ignore the overall scale of  $X$  in our comparisons. To do so, we set  $\sigma_\beta$  such that the trace of the covariance matrix  $\text{tr}(\sigma_\beta^2 X X^T)$  is  $n$ , i.e.  $\sigma_\beta^2 = n \text{tr}^{-1}(X X^T)$ . Setting the trace to any other value by multiplying the  $\sigma_\beta^2$  for all models by the same constant would yield the same distances according to the probability distribution metrics we use here.

The noise variance  $\sigma_\epsilon^2$  is a property of the measurement and should be the same for all models. To keep all our distributions normalized to an average variance of 1 per stimulus, we choose just one parameter  $a \in [0, 1]$  to trade off signal and noise variance, which yields the following distribution for the observations:

$$\mathbf{y} \sim N\left(0, (1-a) \frac{n X X^T}{\text{tr}(X X^T)} + a I\right) \quad (5)$$

We will choose  $a$  depending on the number of images to yield variation in the distances as described below. To justify this, we need to define the distances between distributions we use first though.

### 3.3 Distances between predictive distributions

Here we use two metrics for probability distributions to measure how similar the predictive distributions based on representations are: the Total Variation Distance (TVD) and the Jensen-Shannon Divergence (JSD) [26]. As there are no closed form solutions for computing these distances between Gaussians, we approximate each of them based on  $N = 10\,000$  draws from the respective distributions. For this section we will call the two predictive distributions to be compared  $P_1$  and  $P_2$  with densities  $p_1$  and  $p_2$ .

**Total variation distance** (TVD) is defined as:

$$\text{TVD}(P_1, P_2) = \sup_A |P_1(A) - P_2(A)| \quad (6)$$

For continuous distributions like the Gaussians we deal with here, there are always at least two equivalent  $A$  that maximize the difference:  $A_1 = \{x : p_1(x) > p_2(x)\}$  and  $A_2 = \{x : p_2(x) > p_1(x)\}$ . For each of these we can generate an approximation for the TVD based on samples from  $P_1$  or  $P_2$  respectively: We first note that the density with respect to  $P_1$  of  $P_1$  is 1 and of  $P_2$  is  $\frac{p_2}{p_1}$ . The difference in probabilities for the event that  $p_1 > p_2$  is thus  $\int \max\left(0, 1 - \frac{p_2(x)}{p_1(x)}\right) dP_1(x)$ , which we can approximate with the standard sampling approximation with samples from  $P_1$ . A completely analogous derivation yields an approximation for the probabilities of  $A_2$  based on samples from  $P_2$ . Averaging the two approximations yields the following approximation of the TVD that we used for all computations of the TVD:

$$\text{TVD}(P_1, P_2) \approx \frac{1}{2N} \sum_{i=1}^N \max\left(0, 1 - \frac{p_2(x_i^{(1)})}{p_1(x_i^{(1)})}\right) + \frac{1}{2N} \sum_{i=1}^N \max\left(0, 1 - \frac{p_1(x_i^{(2)})}{p_2(x_i^{(2)})}\right) \quad (7)$$

where  $x^{(1)}$  is a sample of size  $N$  from  $P_1$  and  $x^{(2)}$  is a sample of size  $N$  from  $P_2$ .

**Jensen Shannon Divergence** (JSD) is defined as:

$$\text{JSD}(P_1, P_2) = \int p_1(x) \log_2 \frac{p_1(x)}{p_1(x) + p_2(x)} dx + \int p_2(x) \log_2 \frac{p_2(x)}{p_1(x) + p_2(x)} dx - 1 \quad (8)$$

Where we already pulled out the  $\frac{1}{2}$  from computing the mean in the denominators and used  $\log_2$ , such that the JSD ranges from 0 to 1. The Jensen Shannon Distance is the square root of this value, which is a metric [26]. The two integrals can be approximated with samples from  $P_1$  and  $P_2$  respectively, which yields the approximation we use throughout whenever we need to compute a JSD:

$$\text{JSD}(P_1, P_2) \approx \frac{1}{N} \sum_{i=1}^N \log_2 \frac{p_1(x_i^{(1)})}{p_1(x_i^{(1)}) + p_2(x_i^{(1)})} + \frac{1}{N} \sum_{i=1}^N \log_2 \frac{p_2(x_i^{(2)})}{p_1(x_i^{(2)}) + p_2(x_i^{(2)})} - 1 \quad (9)$$

where  $x^{(1)}$  is a sample of size  $N$  from  $P_1$  and  $x^{(2)}$  is a sample of size  $N$  from  $P_2$ .

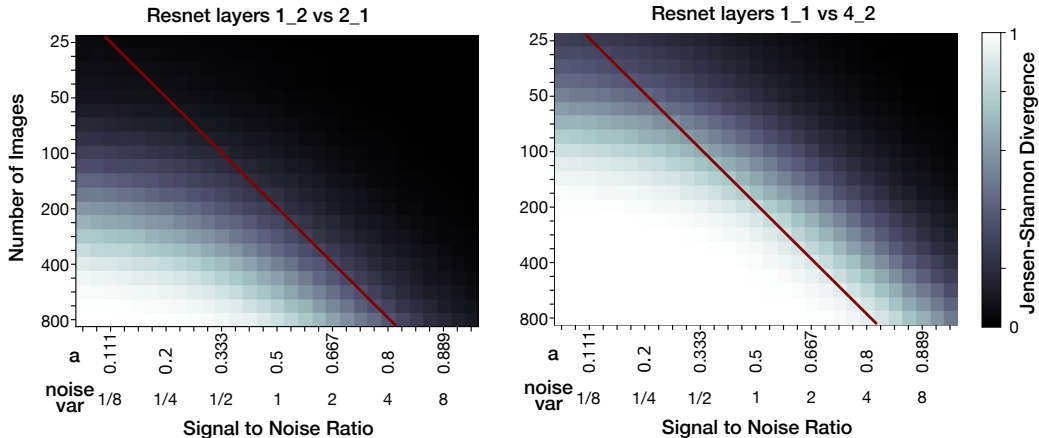


Figure 2: Dependence of the Jensen Shannon Divergence (JSD) on the number of images used and the signal to noise ratio for two comparisons within a standard ResNet-50. For signal to noise ratio we show two labels, the noise variance for signal variance 1 and the mixture factor  $a$  as defined in the text. The red line shows the slope such that the noise variance is proportional to the number of images. Note that JSD is fairly constant along this line once enough images are collected, while JSD gets small for few images independent of the Signal to noise ratio. Left: Divergence between two close representations—the outputs of the first layer and the output of the first block of the second layer. Right: Divergence between to different representations—the first block in the first layer and the last block in the last convolution layer.

**Gradient** We compute both of our distances based on a sum over samples from the two Gaussian distributions. To get a gradient for this function, we can use the reparameterization trick, i.e. we take standard normal samples which are transformed into samples with the right covariance matrix such that our approximation becomes a differentiable function of the covariance matrices and these random samples, allowing us to compute a gradient through our distance [27].

### 3.4 Choosing the signal to noise ratio

When we use more images, representations become easier to discriminate and both TVD and JSD grow (Fig. 2). This makes comparisons with many images uninformative, because all representations become perfectly discriminable and have distances close to 1 to each other. Thus, we adjust the mixture weight for the noise  $a$  to compensate for the number of stimuli.

A sensible dependence between  $a$  and the number of stimuli  $n$  can be derived if we assume that the variance of the noise is proportional to the number of images used. This corresponds to the scaling we get if we repeat measurements of the few images such that we take the same overall number of measurements independent of the number of images and assume the usual  $1/n$  relationship for the noise variance. This yields  $a = \frac{bn}{1+bn}$  where  $b$  is a constant that makes our analysis overall more or less sensitive.

This adjustment of  $a$  does indeed yield a relatively constant level of discriminability once we use enough images for testing (Fig. 2). For small image numbers discriminability tends to fall off independent of the noise variance, even for completely noise free predictions. Based on a few examples, we settled on  $b = 1/100$  such that 100 images yield  $a = 0.5$  for our illustrations. More fine-grained distinctions may profit from using lower noise levels and broader distinctions from even higher noise levels.

### 3.5 Pseudo-metric

For further analyses of the similarities between representations it is advantageous if the similarities are a pseudo-metric on the space of representations [2], because we can then guarantee the convergence and performance of embedding, clustering and other analysis methods.

Our new measures of similarity between representations are pseudo-metrics, because we use metrics to compute the dissimilarity of the predictive distributions. As we have a map from the representation to its predictive distribution this induces a pseudo-metric on the representations, but not a metric, because multiple representations map to the same predictive distribution.

### 3.6 Equivalent representations

Considering some representations to be equivalent is generally desirable, because some representations are indeed completely equivalent. For example, two representations that contain the same features in different orders should be considered the same. There is some discussion on what transformations we should ignore when comparing representations though [2, 28].

To understand what our new metric measures, it is informative to consider which representations are equivalent according to it, i.e. have distance 0 between them. As TVD and JSD are metrics on probability distributions, representations are equivalent if and only if their predictive distributions are the same<sup>2</sup>. For the 0-mean normal distributions we are comparing here, this is equivalent to their covariance matrices being equal. Thus, two representations  $\phi$  and  $\psi$  are equivalent, iff:

$$\frac{X_\psi X_\psi^T}{\text{tr}(X_\psi X_\psi^T)} = \frac{X_\phi X_\phi^T}{\text{tr}(X_\phi X_\phi^T)} \tag{10}$$

The normalization to total variance 1 maps all representations that are scaled by a constant  $k \in \mathbb{R} \setminus \{0\}$  to the same covariance. Thus, representations that differ only by multiplication with a constant are equivalent. Additionally, any unitary or rotation matrix  $U$  such that  $I = UU^T$  applied to the features will yield the same covariance matrix. Formally, if one representation  $X' = XU$  is a rotation of a representation  $X$ , then  $X'X'^T = XU U^T X^T = XX^T$ , i.e. the representations induce the same covariance and are equivalent.

Our new measure does not ignore the norms of the individual patterns or their distance to the origin. The norms determine the predicted variances for the individual stimuli and after normalization the relative sizes of variances are preserved. This is in contrast to representational similarity analysis [23] which analyses only differences between representations and centered kernel alignment, which explicitly removes this information by centering [1]. This also implies that our measure is not invariant to shifts of the representation, i.e. to adding an offset to all representation vectors. This is in contrast to rotation invariant generalized shape metrics, which contain a centering operation which makes them invariant to shifts [2]. Thus our measure is similar to but stricter than existing metrics.

### 3.7 Experiments

We evaluate our methods by comparing deep neural network representations from ImageNet-1k trained models provided with the *torchvision* [29] package in python. As test images, we used randomly chosen unlabeled images from MS COCO [30] from their 'unlabeled2017' folder with a single center crop and the preprocessing required by the respective models. All experiments reported here were run on a single MacBook Pro, M2max with 96Gb of RAM. Single distances are usually computed within less than a second and the longest experiment took 67 minutes of computation time in total. See Appendix A for more details.

## 4 Applications & Results

### 4.1 Example

As an example application, we analyzed the similarities between intermediate representations from 3 standard neural networks based on the Jensen-Shannon-Distance between linear predictions we propose here (Fig. 3). AlexNet [31], ResNet-18 [32] and the Vision Transformer B-16 (ViT-B-16) [33] were obtained from *torchvision* [29] with the standard weights from ImageNet-1k training. Our analysis is based on 200 images from the unlabeled set of MS COCO images and we chose  $a = 2/3$  based on our heuristic (see App. A.1 for more details).

---

<sup>2</sup>Except for a subset of measure 0.

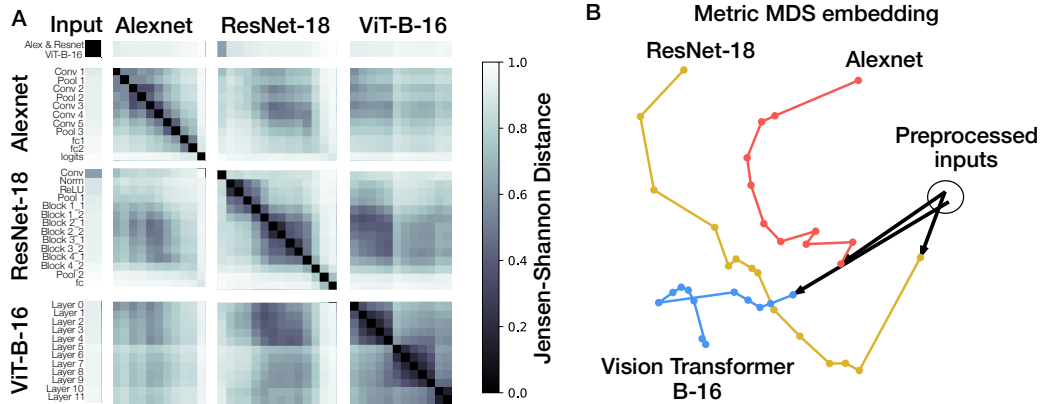


Figure 3: Example analysis based on the Jensen-Shannon Distance we propose here. We compare a range of layers from AlexNet, ResNet-18 and the Vision Transformer B-16 (ViT-B-16) based on 200 randomly chosen natural images. Weights for all networks were obtained from torchvision and were originally trained on ImageNet-1k. **A**: Distance matrix according to our new Jensen-Shannon Distance including the pre-processed input images. **B**: Metric MDS embedding of the layers into a 2D space with arbitrary units.

Our metric yields sensible results. Nearby layers produce similar representations, such that the processing of each network forms a relatively smooth path through the space of representations. The distances fill the full range from 0 to 1 and intermediate representations in different networks show some similarities. We display only the Jensen-Shannon-Distance here, because the two metrics we propose turn out to be very similar in the next section.

We can interpret the behavior of the networks based on the distances: Alexnet takes a relatively unremarkable path through the space of representations from the input images towards the classification output. ResNet-18 first takes a detour with its initial convolution, normalization and pooling operations that are not represented in the other networks, proceeds along a similar trajectory as Alexnet for the convolutional layers and then diverges from it for the final classification. The Vision Transformer (ViT-B-16) follows a different trajectory that can be separated into three fairly discrete steps: It first jumps to a representation that is similar to the representations Alexnet and Resnet-18 agree on and moves little for 4 more encoder blocks. Then it jumps to a second cluster of another 5 similar representations and finally creates two more representations similar representations. Overall, the transformer’s representations move away from Alexnet and Resnet-18 with each jump.

Analyses like these can be very informative for understanding how networks process their inputs. The Vision Transformer (ViT-B-16) is a particular interesting example, because the encoder blocks all have the same internal architecture, i.e. the steps between the clusters of representations have no correspondence to any change in the architecture of the network.

## 4.2 Comparison to other metrics

To compare our two metrics to each other and to other measures of dissimilarity of neural network representations, we ran an analysis comparing all layers of AlexNet and ResNet-50 to each other (Fig. 4). Here we used 100 random samples of 100 images each from the first 1000 unlabeled images of MS COCO as test stimuli and display the mean across image samples (more details in Appendix A.3). In broad strokes the metrics all agree: Close-by neural network layers tend to be similar to each other; some of the intermediate convolutional layers produce similar representations in the two networks; and the final readout layers of both networks are very different from the convolutional layers.

Our two different metrics between probability distributions yield extremely similar results (Pearson correlation  $r(198) = 0.99980$ ). Thus, for all intents and purposes the two metrics are equivalent. They are not exactly the same though. The Total Variation Distance is systematically ever so slightly smaller for intermediate values and this difference is larger than our numerical errors.

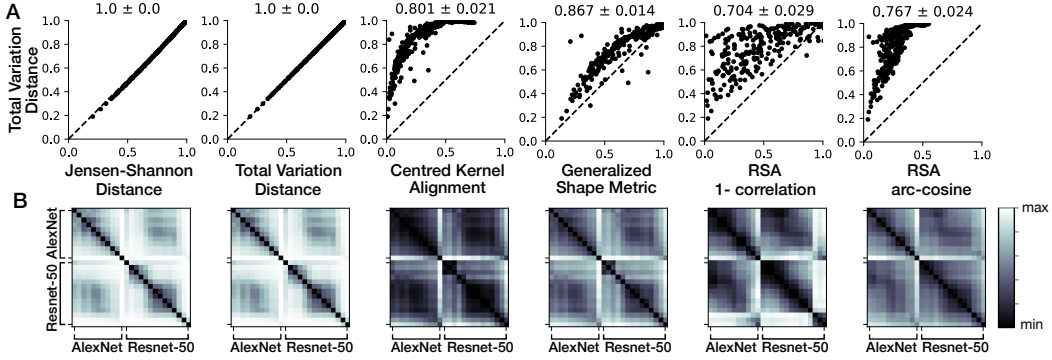


Figure 4: Comparisons between metrics based on all pairwise distances between layers of Alexnet and Resnet-50 using 100 random unlabeled images from MS COCO as inputs. **A:** Plotting different dissimilarity measures against the total variation distance we propose here. The number above each plot gives the Pearson correlation  $\pm$  the coarse analytic estimate of the standard deviation  $(1-r^2)/\sqrt{N-3}$  [34]. **B:** The matrix of pairwise comparisons between layers according to the different dissimilarity measures. **Compared measures:** Jensen-Shannon-Distance & Total variation distance as proposed here. Centred Kernel Alignment: One minus the linear centered kernel alignment. Generalized Shape Metric: arccos of the centered kernel alignment, which is a shape metric [2, Appendix C.7]. RSA 1-correlation: Representational similarity analysis based on one minus the Pearson correlation of euclidean distances. RSA arc-cosine: Representational similarity analysis based on the arccos of the cosine similarity of euclidean distances.

The other metrics also show fairly strong relationships with our newly proposed metrics. In particular, the arccos of the centered kernel alignment [1] as suggested by [2] shows a fairly close relationship. The non-metric measures show bigger differences from our new metrics and the RSA measures are least similar to our new metrics. In general, existing metrics are also less stringent, i.e. the distances between layers are smaller according to existing metrics than according to our new one, which fits our observations about which representations are equivalent.

### 4.3 Stability analysis

We need to characterize how variable the results of our analyses are to know how confident we should be in our results. The variability of our results depend on the amount of test data we use of course which complicates this judgment.

**Number of Images** Different test images will yield different distances between layers. This is probably the largest source of variability for noiseless representations. To understand how much variance this causes we analyzed the repeats of the simulations we used for comparisons to other metrics above (Tab. 1). The variance of estimates depends substantially on the mean distance value and the mean are different for different image numbers and different metrics. For this reason, we believe the maximum and median standard deviations are more informative than mean standard deviations and we should nonetheless be careful when interpreting these values.

Nonetheless, we can make three observations. First, the standard deviations we observe are reasonably small for most metrics and decrease at least as fast as expected ( $1/\sqrt{n}$  with the number of test images). Second, our new metrics are at least as stable as existing ones, perhaps a little more so. Third, the correlation distance of RSA varies far more than other metrics, by more than a factor 10 in variance. Thus, our metrics are certainly competitive in terms of stability, but the correlation distance between representational dissimilarity matrices should not be used for comparisons between DNN layers.

**Number of samples** We approximate the distances we use based on sampling approximations to the integrals that occur. This creates an approximation error. We can estimate the size of this error from the variance of the averaged values (see App. A.4 for details). For both our metrics, the dependence between variance and the true distance was independent of the number of stimuli and the dimensionality of the representations. It is inverse-u-shaped with the variance approaching 0 at



Table 1: Standard deviations of the distance measures across different image choices based on 100 random image samples each. Each cell shows maximum / median across the 300 distances among the 25 layers of AlexNet and ResNet-50 we used for comparisons. See Fig. 4 for details on the metrics.

med / max	JSD	TVD	CKA	Shape Metric	RSA 1-corr	RSA arccos
$n = 25$	0.029/0.068	0.029/0.069	0.027/0.056	0.051/0.094	0.144/0.246	0.041/0.079
$n = 50$	0.017/0.055	0.018/0.055	0.021/0.044	0.037/0.077	0.103/0.182	0.031/0.068
$n = 100$	0.008/0.034	0.009/0.035	0.016/0.034	0.025/0.055	0.070/0.135	0.021/0.049

0 and 1 and the peak at about 0.6 for total variation distance and 0.5 Jensen-Shannon Divergence. The maximum variance is about  $\frac{0.339}{N}$  for Jensen-Shannon Divergence ( $SD(N = 10\,000) \approx 0.0058$ ) and about  $\frac{0.071}{N}$  for total variation distance ( $SD(N = 10\,000) \approx 0.0027$ ). Due to the square root transform the analysis for the Jensen-Shannon distance is a little more involved, but also turns out fine (see App. A.4). Thus, we deemed 10 000 samples from each distribution to be sufficient. When many hundreds of test inputs are used, higher sample numbers may be justified to keep the variance due to the approximation small compared to the variability caused by input choice.

## 5 Discussion

We present a new measure for the similarity of representations based on Bayesian statistics. Our new measure is a (pseudo-) metric for representations, compares predictions for a linear readout, directly quantifies how well representations can be discriminated based on a linear readout, can be computed from the linear kernel matrix of the representation including a stochastic gradient, and nicely unifies existing methods for comparing representations. Total variation distance and Jensen-Shannon distance give very similar results, but the numerical approximation is more stable and efficient for the total variation distance. Thus, we recommend using the total variation distance.

Our metrics quantify how well the representations can be differentiated based on a linear readout: The Jensen-Shannon distance the information gain for probabilistic inference and the total variation distance the accuracy of hard decision boundary. Thus, our distances are also interesting for the design of neuroscience experiments. Analyses like the ones in Fig. 2 are effectively a power analysis based on the chosen stimuli and the signal to noise ratio. The connection to discriminability and the (stochastic) gradient make our metric an ideal target for stimulus optimization techniques as well (e.g. [35]). We should perhaps consider using Bayesian inference for the final comparison of models, too. Bayesian inference for this linear model is analytically tractable for up to 1 000s of stimuli, independent of the dimensionality of the representations and provides an estimate of uncertainty about the weights and the predictions for specific images due to insufficient training data.

Overall, our new metrics are a great extension of our toolkit for comparing representations. Our metrics are well justified on a theoretical level, provide novel statistical interpretations and work well in practice. They differentiate more representations than centered kernel alignment or representational similarity analysis, but they are still invariant to rotations of the representations.

## 6 Limitations

As most measures of similarity, our new measure depends on the stimuli chosen for the comparison. If there is a population of stimuli we can justify generalization to this population using established statistical inference schemes [13]. Thus, it is not fundamental whether we describe our distances as dependent on the sample we took or on the population of stimuli we sampled from. One of the two should be described whenever we compare networks though as the similarities might be fundamentally different depending on whether we use clean images, images distorted by noise, or adversarial examples for example.

All results in this paper concern image classification models as this is our area of expertise and among the most common types of deep neural network. We see no reason why our methods should be restricted to image processing models though. As long as we can process a set of different stimuli and think of a linear probe into internal representations, our methods should apply.

The computations we describe here run fairly quickly, but are based on the stimulus  $\times$  stimulus kernel matrix such that memory requirements scale quadratically with the number of images used and computations are of cubic complexity due to a Cholesky decomposition of the covariance matrices. In practice, this restricts our measures to situations with at most 1000s of images. This number is sufficient for most linear probe tasks and batch-sizes used for deep neural networks, but we cannot compute similarities based on complete deep learning datasets.

## References

- [1] Simon Kornblith, Mohammad Norouzi, Honglak Lee, and Geoffrey Hinton. Similarity of neural network representations revisited. In *International conference on machine learning*, pages 3519–3529. PMLR, 2019.
- [2] Alex H Williams, Erin Kunz, Simon Kornblith, and Scott Linderman. Generalized shape metrics on neural representations. *Advances in Neural Information Processing Systems*, 34:4738–4750, 2021.
- [3] Behnam Neyshabur, Hanie Sedghi, and Chiyuan Zhang. What is being transferred in transfer learning? *Advances in neural information processing systems*, 33:512–523, 2020.
- [4] Aniruddh Raghu, Maithra Raghu, Samy Bengio, and Oriol Vinyals. Rapid learning or feature reuse? towards understanding the effectiveness of maml. *arXiv preprint arXiv:1909.09157*, 2019.
- [5] Maithra Raghu, Thomas Unterthiner, Simon Kornblith, Chiyuan Zhang, and Alexey Dosovitskiy. Do vision transformers see like convolutional neural networks? *Advances in neural information processing systems*, 34:12116–12128, 2021.
- [6] Lin Wang and Kuk-Jin Yoon. Knowledge Distillation and Student-Teacher Learning for Visual Intelligence: A Review and New Outlooks. *IEEE Transactions on Pattern Analysis and Machine Intelligence*, 44(6):3048–3068, June 2022. ISSN 0162-8828, 2160-9292, 1939-3539. doi: 10.1109/TPAMI.2021.3055564. URL <http://arxiv.org/abs/2004.05937>. arXiv:2004.05937 [cs].
- [7] Nikolaos Passalis and Anastasios Tefas. Learning Deep Representations with Probabilistic Knowledge Transfer. In Vittorio Ferrari, Martial Hebert, Cristian Sminchisescu, and Yair Weiss, editors, *Computer Vision – ECCV 2018*, volume 11215, pages 283–299. Springer International Publishing, Cham, 2018. ISBN 978-3-030-01251-9 978-3-030-01252-6. doi: 10.1007/978-3-030-01252-6\_17. URL [https://link.springer.com/10.1007/978-3-030-01252-6\\_17](https://link.springer.com/10.1007/978-3-030-01252-6_17). Series Title: Lecture Notes in Computer Science.
- [8] Jörn Diedrichsen, Gerard R. Ridgway, Karl J. Friston, and Tobias Wiestler. Comparing the similarity and spatial structure of neural representations: A pattern-component model. *NeuroImage*, 55(4):1665–1678, April 2011. ISSN 1053-8119. doi: 10.1016/j.neuroimage.2011.01.044. URL <http://www.sciencedirect.com/science/article/pii/S1053811911000796>.
- [9] Jörn Diedrichsen and Nikolaus Kriegeskorte. Representational models: A common framework for understanding encoding, pattern-component, and representational-similarity analysis. *PLOS Computational Biology*, 13(4):e1005508, April 2017. ISSN 1553-7358. doi: 10.1371/journal.pcbi.1005508. URL <http://journals.plos.org/ploscompbiol/article?id=10.1371/journal.pcbi.1005508>.
- [10] Seyed-Mahdi Khaligh-Razavi, Linda Henriksson, Kendrick Kay, and Nikolaus Kriegeskorte. Fixed versus mixed RSA: Explaining visual representations by fixed and mixed feature sets from shallow and deep computational models. *Journal of Mathematical Psychology*, 76: 184–197, February 2017. ISSN 0022-2496. doi: 10.1016/j.jmp.2016.10.007. URL <http://www.sciencedirect.com/science/article/pii/S0022249616301134>.
- [11] Thomas Naselaris, Kendrick N. Kay, Shinji Nishimoto, and Jack L. Gallant. Encoding and decoding in fMRI. *NeuroImage*, 56(2):400–410, May 2011. ISSN 10538119. doi: 10.1016/j.neuroimage.2010.07.073. URL <https://linkinghub.elsevier.com/retrieve/pii/S1053811910010657>. Number: 2.

- [12] Katherine R. Storrs, Tim C. Kietzmann, Alexander Walther, Johannes Mehrer, and Nikolaus Kriegeskorte. Diverse Deep Neural Networks All Predict Human Inferior Temporal Cortex Well, After Training and Fitting. *Journal of Cognitive Neuroscience*, pages 1–21, August 2021. ISSN 1530-8898. doi: 10.1162/jocn\_a\_01755. URL [https://direct.mit.edu/jocn/article/doi/10.1162/jocn\\_a\\_01755/103001/Diverse-Deep-Neural-Networks-All-Predict-Human](https://direct.mit.edu/jocn/article/doi/10.1162/jocn_a_01755/103001/Diverse-Deep-Neural-Networks-All-Predict-Human).
- [13] Heiko H Schütt, Alexander D Kipnis, Jörn Diedrichsen, and Nikolaus Kriegeskorte. Statistical inference on representational geometries. *eLife*, 12:e82566, 2023. ISSN 2050-084X. doi: 10.7554/eLife.82566. URL <https://doi.org/10.7554/eLife.82566>. Publisher: eLife Sciences Publications, Ltd tex.article\_type: journal tex.citation: eLife 2023;12:e82566 tex.pub\_date: 2023-08-23.
- [14] Radoslaw Martin Cichy, Gemma Roig, Alex Andonian, Kshitij Dwivedi, Benjamin Lahner, Alex Lascelles, Yalda Mohsenzadeh, Kandan Ramakrishnan, and Aude Oliva. The Algonauts Project: A Platform for Communication between the Sciences of Biological and Artificial Intelligence, May 2019. URL <http://arxiv.org/abs/1905.05675>. Issue: arXiv:1905.05675 arXiv:1905.05675 [cs, q-bio].
- [15] Martin N. Hebart, Adam H. Dickter, Alexis Kidder, Wan Y. Kwok, Anna Corriveau, Caitlin Van Wicklin, and Chris I. Baker. THINGS: A database of 1,854 object concepts and more than 26,000 naturalistic object images. *PLOS ONE*, 14(10):e0223792, October 2019. ISSN 1932-6203. doi: 10.1371/journal.pone.0223792. URL <https://dx.plos.org/10.1371/journal.pone.0223792>. Number: 10.
- [16] Martin Schrimpf, Jonas Kubilius, Michael J. Lee, N. Apurva Ratan Murty, Robert Ajemian, and James J. DiCarlo. Integrative Benchmarking to Advance Neurally Mechanistic Models of Human Intelligence. *Neuron*, 108(3):413–423, November 2020. ISSN 08966273. doi: 10.1016/j.neuron.2020.07.040. URL <https://linkinghub.elsevier.com/retrieve/pii/S089662732030605X>.
- [17] Robert Geirhos, David H. J. Janssen, Heiko H. Schütt, Jonas Rauber, Matthias Bethge, and Felix A. Wichmann. Comparing deep neural networks against humans: object recognition when the signal gets weaker. *arXiv:1706.06969 [cs, q-bio, stat]*, December 2018. URL <http://arxiv.org/abs/1706.06969>. arXiv: 1706.06969.
- [18] Robert Geirhos, Carlos R M Temme, Jonas Rauber, Heiko H Schütt, Matthias Bethge, and Felix A Wichmann. Generalisation in humans and deep neural networks. In *Advances in neural information processing systems*, volume 31, page 13. Curran Associates, Inc., 2018. URL <https://proceedings.neurips.cc/paper/2018/file/0937fb5864ed06ffb59ae5f9b5ed67a9-Paper.pdf>.
- [19] Guillaume Alain and Yoshua Bengio. UNDERSTANDING INTERMEDIATE LAYERS USING LINEAR CLASSIFIER PROBES. 2017.
- [20] Enric Boix-Adsera, Hannah Lawrence, George Stepaniants, and Philippe Rigollet. GULP: a prediction-based metric between representations. In *Advances in Neural Information Processing Systems*, volume 35, pages 7115–7127, 2022. URL <http://arxiv.org/abs/2210.06545>.
- [21] David R. Hardoon, Sandor Szedmak, and John Shawe-Taylor. Canonical correlation analysis: An overview with application to learning methods. *Neural Computation*, 16(12):2639–2664, 2004. doi: 10.1162/0899766042321814.
- [22] Maithra Raghu, Justin Gilmer, Jason Yosinski, and Jascha Sohl-Dickstein. SVCCA: Singular Vector Canonical Correlation Analysis for Deep Learning Dynamics and Interpretability. *arXiv:1706.05806 [cs, stat]*, November 2017. URL <http://arxiv.org/abs/1706.05806>. arXiv: 1706.05806.
- [23] Nikolaus Kriegeskorte, Marieke Mur, and Peter A. Bandettini. Representational similarity analysis - connecting the branches of systems neuroscience. *Frontiers in Systems Neuroscience*, 2, 2008. ISSN 1662-5137. doi: 10.3389/neuro.06.004.2008. URL <https://www.frontiersin.org/articles/10.3389/neuro.06.004.2008/full>.

- [24] Jörn Diedrichsen, Eva Berlot, Marieke Mur, Heiko H. Schütt, Mahdiyar Shahbazi, and Nikolaus Kriegeskorte. Comparing representational geometries using whitened unbiased-distance-matrix similarity. *Neurons, Behavior, Data analysis, and Theory*, 5(3), 2021. doi: 10.51628/001c.27664. URL <https://doi.org/10.51628/001c.27664>. Number: 3.
- [25] Sarah E. Harvey, Brett W. Larsen, and Alex H. Williams. Duality of Bures and Shape Distances with Implications for Comparing Neural Representations, November 2023. URL <http://arxiv.org/abs/2311.11436>. arXiv:2311.11436 [cs, stat].
- [26] D.M. Endres and J.E. Schindelin. A new metric for probability distributions. *IEEE Transactions on Information Theory*, 49(7):1858–1860, July 2003. ISSN 0018-9448. doi: 10.1109/TIT.2003.813506. URL <http://ieeexplore.ieee.org/document/1207388/>. Number: 7.
- [27] Diederik P. Kingma and Max Welling. Auto-Encoding Variational Bayes. *arXiv:1312.6114 [cs, stat]*, December 2013. URL <http://arxiv.org/abs/1312.6114>. arXiv: 1312.6114.
- [28] Nikolaus Kriegeskorte and Jörn Diedrichsen. Peeling the Onion of Brain Representations. *Annual Review of Neuroscience*, 42(1):407–432, July 2019. ISSN 0147-006X, 1545-4126. doi: 10.1146/annurev-neuro-080317-061906. URL <https://www.annualreviews.org/doi/10.1146/annurev-neuro-080317-061906>. Number: 1.
- [29] TorchVision maintainers and contributors. TorchVision: PyTorch’s computer vision library, 2016. URL <https://github.com/pytorch/vision>.
- [30] Tsung-Yi Lin, Michael Maire, Serge Belongie, Lubomir Bourdev, Ross Girshick, James Hays, Pietro Perona, Deva Ramanan, C. Lawrence Zitnick, and Piotr Dollár. Microsoft COCO: Common Objects in Context. *arXiv:1405.0312 [cs]*, February 2015. URL <http://arxiv.org/abs/1405.0312>. arXiv: 1405.0312.
- [31] Alex Krizhevsky, Ilya Sutskever, and Geoffrey E. Hinton. Imagenet classification with deep convolutional neural networks. In *Advances in neural information processing systems*, pages 1097–1105, 2012.
- [32] Kaiming He, Xiangyu Zhang, Shaoqing Ren, and Jian Sun. Deep Residual Learning for Image Recognition. In *2016 IEEE Conference on Computer Vision and Pattern Recognition (CVPR)*, pages 770–778, Las Vegas, NV, USA, June 2016. IEEE. ISBN 978-1-4673-8851-1. doi: 10.1109/CVPR.2016.90. URL <http://ieeexplore.ieee.org/document/7780459/>.
- [33] Alexey Dosovitskiy, Lucas Beyer, Alexander Kolesnikov, Dirk Weissenborn, Xiaohua Zhai, Thomas Unterthiner, Mostafa Dehghani, Matthias Minderer, Georg Heigold, Sylvain Gelly, Jakob Uszkoreit, and Neil Houlsby. AN IMAGE IS WORTH 16X16 WORDS: TRANSFORMERS FOR IMAGE RECOGNITION AT SCALE. *International conference on learning representations (ICLR)*, 2021. URL <https://openreview.net/pdf?id=YicbFdNTTy>.
- [34] Timo Gnams. A Brief Note on the Standard Error of the Pearson Correlation. *Collabra: Psychology*, 9(1):87615, September 2023. ISSN 2474-7394. doi: 10.1525/collabra.87615. URL <https://online.ucpress.edu/collabra/article/9/1/87615/197169/A-Brief-Note-on-the-Standard-Error-of-the-Pearson>.
- [35] Tal Golan, Prashant C. Raju, and Nikolaus Kriegeskorte. Controversial stimuli: Pitting neural networks against each other as models of human cognition. *Proceedings of the National Academy of Sciences*, 117(47):29330–29337, November 2020. ISSN 0027-8424, 1091-6490. doi: 10.1073/pnas.1912334117. URL <https://pnas.org/doi/full/10.1073/pnas.1912334117>.
- [36] Adam Paszke, Sam Gross, Francisco Massa, Adam Lerer, James Bradbury, Gregory Chanan, Trevor Killeen, Zeming Lin, Natalia Gimelshein, Luca Antiga, Alban Desmaison, Andreas Köpf, Edward Yang, Zach DeVito, Martin Raison, Alykhan Tejani, Sasank Chilamkurthy, Benoit Steiner, Lu Fang, Junjie Bai, and Soumith Chintala. PyTorch: An Imperative Style, High-Performance Deep Learning Library, December 2019. URL <http://arxiv.org/abs/1912.01703>. arXiv:1912.01703 [cs, stat].

- [37] Alex Krizhevsky. One weird trick for parallelizing convolutional neural networks, April 2014. URL <http://arxiv.org/abs/1404.5997>. arXiv:1404.5997 [cs].
- [38] Olga Russakovsky, Jia Deng, Hao Su, Jonathan Krause, Sanjeev Satheesh, Sean Ma, Zhiheng Huang, Andrej Karpathy, Aditya Khosla, Michael Bernstein, Alexander C. Berg, and Li Fei-Fei. ImageNet Large Scale Visual Recognition Challenge. *arXiv:1409.0575 [cs]*, September 2014. URL <http://arxiv.org/abs/1409.0575>. arXiv: 1409.0575.
- [39] F. Pedregosa, G. Varoquaux, A. Gramfort, V. Michel, B. Thirion, O. Grisel, M. Blondel, P. Prettenhofer, R. Weiss, V. Dubourg, J. Vanderplas, A. Passos, D. Cournapeau, M. Brucher, M. Perrot, and E. Duchesnay. Scikit-learn: Machine learning in Python. *Journal of Machine Learning Research*, 12:2825–2830, 2011.
- [40] Alexander Walther, Hamed Nili, Naveed Ejaz, Arjen Alink, Nikolaus Kriegeskorte, and Jörn Diedrichsen. Reliability of dissimilarity measures for multi-voxel pattern analysis. *NeuroImage*, 137:188–200, August 2016. ISSN 10538119. doi: 10.1016/j.neuroimage.2015.12.012. URL <https://linkinghub.elsevier.com/retrieve/pii/S1053811915011258>.

## A Appendix: Experiment details

**Test images** The experiments we describe in the paper were all performed based on the unlabeled images from MS COCO [30]. They are provided by the COCO consortium at <http://images.cocodataset.org/zips/unlabeled2017.zip>. The annotation information for these images is licensed under a CC BY 4.0 license. The individual images were taken by a variety of flickr users and licenses under a range of different CC licenses. The license information for each image is available at [http://images.cocodataset.org/annotations/image\\_info\\_unlabeled2017.zip](http://images.cocodataset.org/annotations/image_info_unlabeled2017.zip).

**Networks** We used three networks as implemented in the torchvision.models module version 0.15.2 [29] with pytorch version 2.1.0 [36].

The first network was Alexnet [31, 37], for which we used the "IMAGENET1K\_V1" weights, which were trained on ImageNet-1k [38]. For all convolutional and fully connected layers we used the representations after the non-linearity and included all layers in the comparison.

The second network was ResNet-18 [32] with "IMAGENET1K\_V1" weights also trained on ImageNet-1k [38]. This networks architecture is primarily based on 4 main layers which each contain two residual blocks. We included all layers before and after the 4 layers and outputs of the two residual blocks for each main layer.

The third network was the Vision Transformer ViT-B-16 [33] also with "IMAGENET1K\_V1" weights. For this network we include the 12 encoder layers outputs. This network uses a slightly different preprocessing procedure than the other two networks, which causes the difference in preprocessed input locations in Figure 3.

**precompute** To speed up simulations, we precomputed the inner product matrix for all network layers for the first 1000 images from the image set and took subsets of those to compute the distances. All simulations below are based on this set of 1000 images. Precomputing these inner product matrices takes only a couple of minutes on the laptop, but removing the interaction with the neural networks from the analysis code simplifies it substantially.

### A.1 Example

For our example analysis presented in Figure 3, we computed our Jensen-Shannon divergence based metric for each pair of layers from all three networks and also compared to the pixel values of the preprocessed images. AlexNet and ResNet-18 use the same preprocessing, but the vision transformer uses a slightly different one, which causes two rows of divergences for the inputs.

To create the MDS embedding we used sci-kit learn [39] with the square root of the Jensen-Shannon Divergence as a precomputed distance metric.

### A.2 Choosing $a$

For choosing the signal to noise ratio or  $a$ , we looked at a range of distances and computed the distance with different numbers of images and signal to noise ratios. Two of those simulations are displayed in Figure 2. The images for this simulation were always the first  $n$  images from the unlabeled images from MS COCO as described above. The displayed comparisons were chosen from the matrix of comparisons between all Alexnet layers and all ResNet-18 layers, but both displayed comparisons remained within ResNet-18.

### A.3 Comparisons between metrics

To compare to other metrics and analyze the stability of metrics we ran 100 repetitions each with a random image sample from the 1000 precomputed images. We varied the number of images used using 25, 50 or 100 images. Figure 4 shows the average results for the 100 images case and Table 1 summarizes the standard deviations we observed across the 100 repetitions. This analysis took the most computation of all experiments for this paper at 67 minutes of computation time on the MacBook pro M2Max laptop.

To enable direct comparisons, we implemented all measures of dissimilarity as functions of the inner product matrix  $XX^T$  and transform them such that large values correspond to very different representations as follows:

**Jensen Shannon Divergence** was computed as described in the main text. For comparisons, we applied a square root to all values to get values that actually are a metric.

**Total Variation Distance** was computed as described in the main text and not transformed in any way.

**Centered Kernel Alignment** is naturally a function of the inner product / kernel matrices [1]. We only use linear centered kernel alignment here. We transform the values we get by taking one minus the value to transform this such that large values correspond large differences instead of large alignment.

**Generalized Shape Metric** is a particular generalized shape metric that can be computed from the kernel matrix according to [2], described in their Appendix C.7. It is computed as the arccos of the centered kernel alignment. This conveniently already transforms the value into a metric with 0 corresponding to equivalence and 1 corresponding to the maximal distance. As noted in [24], centered kernel alignment is equivalent to representational similarity analysis with a special whitened cosine measure for the similarity of dissimilarity matrices, giving another justification for this measure.

**Representational Similarity Analysis** is based on a dissimilarity matrix. Fortunately, euclidean distance is easy to compute from the inner product matrix: The squared euclidean distance from  $x_i$  to  $x_j$  is:  $\|x_i - x_j\|^2 = (x_i - x_j)^T(x_i - x_j) = x_i^T x_i + x_j^T x_j - 2x_i^T x_j$ . We use this formula to convert the kernel matrix into a squared euclidean distance matrix. Then we compute one minus the Pearson correlation of the upper triangular part of this matrix. This realizes one of many possible measures for similarity from representational similarity analysis [40].

**Representational Similarity Analysis:** arccos Here, we measure similarity using the cosine similarity of the upper triangular part of the distance matrix instead of the correlation [24]. We transform the resulting value into a distance measure by applying an arccos to the values. Effectively this process computes the angle between the distance vectors. Among other things, this makes this measure a metric on distance matrices, which induces a (pseudo-)metric on representations.

#### A.4 Numerical stability

**Number of Images** For this analysis we analyzed the variability across image samples from the comparisons between metrics.

**Number of Samples** To estimate the variance of our estimates due to the sampling approximation, we note that both of our approximations are simple averages over samples. Thus, the variance is simply the variance of the samples divided by the number of samples.

We used the first 100 images from the unlabeled set from MS COCO as described above, based on the precomputed inner product matrices and used 10 000 samples for each distance to compute the variance from the values. Computing these distances for all pairs of layers takes about 5 minutes on the MacBook pro M2Max of the first author.

Both metrics show a inverse u shaped relationship of variance on distance (Fig. 5). In the main text we report the maximum of these variances. It is clear from the scale that the estimation of total variation distances is substantially more accurate than the one of the Jensen-Shannon Divergence.

To compute a metric we often compute the square root of the Jensen-Shannon Divergence, which looks problematic at first glance, because the square root function's derivative diverges at 0. One could fear that the variance of the distance (Fig. 5 C) diverges at 0. This means that we require an argument to show that our approximation converges and always has finite variance that converges to 0.

Formally we can start with the statement that the distance estimate has finite variance. This is readily apparent because our distance estimate is always in  $[0, 1]$  and thus must have variance  $\leq 0.25$ . Further,

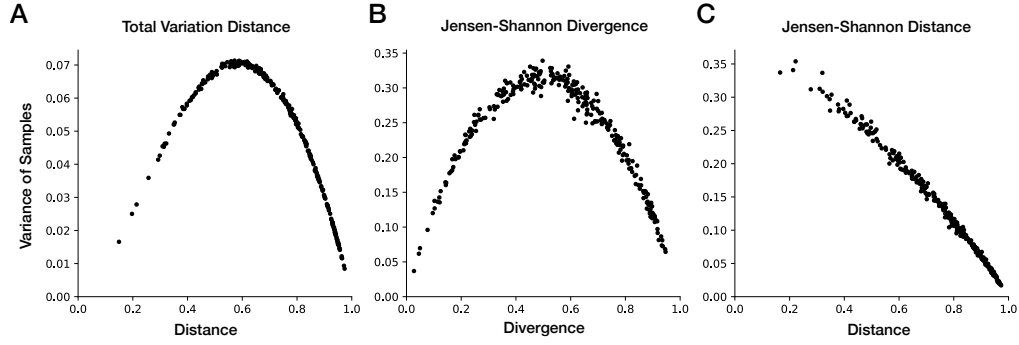


Figure 5: Detailed numerical stability results on numerical stability of the sampling approximations. Variance of samples is the correct sum of variances such that the variance of the estimator becomes this value divided by the number of samples taken. The different points each correspond to one pair of layers and is estimated based on 100 images and 10000 samples. **A & B**: untransformed estimates of the total variation distance and the Jensen-Shannon Divergence. **C**: Jensen-Shannon *distance*, i.e. the square root of the Jensen Shannon divergence. For the distance this is the simple approximation computed by dividing the estimate by the squared derivative of the square-root transformation.

the mean of our samples converges to the true value in probability. Thus, the distance also converges in probability to the correct value. Convergence in probability means that we can choose an  $\epsilon$  range around the true value which will occur with high probability  $1 - \alpha$  for all sample numbers  $N \geq N_0$ . For such  $N$  the variance of the distance estimate must then be smaller than  $(1 - \alpha)\epsilon^2 + 0.25\alpha$ , which we can make arbitrarily small by choosing  $\alpha$  and  $\epsilon$  small enough. Thus the variance converges to 0.